ELSEVIER

Catalysis Today 58 (2000) 115–123

CATALYSIS TODAY

www.elsevier.com/locate/cattod

Scaling properties in photocatalysis

Micha Tomkiewicz

Department of Physics, Brooklyn College of the City, University of New York, Brooklyn, New York, NY 11210, USA

Abstract

In this paper we will try to demonstrate that in nanostructured materials the scaling of many of the material properties that are important for catalytic activity diverges as one approaches nanosize dimensions. We will discuss size-induced critical properties that include transport, polarizability and adsorption properties. The macroscopic context will be demonstrated in terms of three main applications of nanocrystalline, semiconducting, photocatalytic materials with particular emphasis on nanocrystalline TiO_2. These applications include: liquid-junction photovoltaic solar cells; photodecomposition of organic compounds with nanocrystalline photocatalysts and light-induced wetting properties.

Keywords: Photochemistry; Nanocrystalline; TiO_2

1. Introduction

Arguably the 1990s will be characterized as the beginning of the nano decade [1]. To a large degree the large effort in nanoscience stems from progress in surface probe microscopies [2] that enables researchers to synthesize, observe and characterize on the nanostructure level. The literature is immersed with great number of excellent review articles that summarize various aspects of the field [3]. Photochemistry and photophysics with nanostructure materials are of particular interest since the light absorption and the initial charge separation takes place on a single particle level while the system responds with macroscopic output characteristics in which all the length scales that were used to describe such systems are considerably larger than the single particle size. The scaling properties of photocatalytic systems that will correlate the macroscopic properties with single particle properties through the morphology of the systems is an area that is still in its infancy. Traditionally, the variation of catalytic properties with particle size was associated with the increase in the specific area and the corresponding increase of available active sites [4]. It was long realized that the simple correlation with surface area will evolve into a diffusion-limited process in which pore structure will determine the kinetics as the rate of the reaction increases. Morphologies in the nanostructure regime are not different, the balance between active surface area and efficient diffusion that will contribute to the overall rate is as valid as for larger-particle size systems. However, some phenomena are emerging that have strong influence on the catalytic reactions that are correlated with the nano-size and have no equivalent in larger particles.

Zeolites are probably the most widely used commercial catalysts. The world market total of synthetic zeolites is approximated at 1.5 billion dollars [5]. The zeolites are crystalline aluminosilicates with a three-dimensional framework of pores with a uniform diameter that encloses internal cavities and channels

Email address: michatom@brooklyn.cuny.edu (M. Tomkiewicz)

0920-5861/00/$ – see front matter
PII: S0920-5861(00)00246-7

of discrete size and shape that permit selective adsorption and separation. The principal applications are in detergents, and petroleum cracking. In a recent review [6], the specific properties of this class of catalysts that account for their wide use was summarized as follows:

1. They have very high surface area and adsorption capacity.
2. The adsorption properties of the zeolites can be controlled, and they can be varied from hydrophobic to hydrophilic type materials.
3. Active sites, such as acid sites for instance, can be generated in the framework and their strength and concentration can be tailored for a particular application.
4. The sizes of their channels and cavities are in the range typical for many molecules of interest (5–12 Å), and the strong electric fields existing in those micropores together with an electronic confinement of the guest molecules are responsible for a activation of the reactants.
5. Their intricate channel structure allows the zeolites to present different types of shape selectivity, i.e., product, reactant, and transition state, which can be used to direct a given catalytic reaction toward the desired product avoiding undesired side reactions.

In addition, the materials are stable at high temperature in a large variety of chemical environments.

In this paper, we will try to demonstrate that in nanostructured materials, the scaling of many of the material properties that are important for catalytic activity diverges as one approaches nanosize dimensions. This offers the premise of broadening the scope of materials for catalytic applications, and in particular materials with optical properties that will make them useful for photocatalytic applications. Attempts to combine the properties of zeolites with the photoactivity of guest materials can be found mainly in the work of Calzaferri et al. [7].

Currently, photocatalytic applications are aimed at three principal directions: photocatalytic chemistry, photovoltaic applications and wettability.

This paper is organized by first describing the three main applications of nanocrystalline semiconducting photocatalysts followed by description of size-induced critical properties that include transport, polarizability and adsorption properties. We will not discuss here the scaling properties of the optical properties that emerges from confinement, because this topic is extensively covered in the literature [8–10].

2. Liquid-junction photovoltaic solar cells with nanocrystalline semiconductors

The work by O'Regan and Grätzel [11] have demonstrated that high power conversion efficiency and stability can be attained by dye-sensitized photoelectrochemical photovoltaic cells that are based on nanocrystalline porous TiO_2 that are sensitized by Ru-containing metal-organic dye complexes. Since this announcement, a considerable amount of work has been conducted throughout the world, first to confirm the results [12] and then to try to improve and understand the physics and chemistry that takes place in these systems [13–15]. Schematic representation of such a cell is shown in Fig. 1. Light is absorbed by the dye separating an electron–hole pair. Time resolved measurements clearly demonstrate that electron transfer takes place from the photoexcited dye to the TiO_2 nanoparticle. [16–18]. The time scale for this transfer is reported to be faster than 50 fs [16]. This negatively

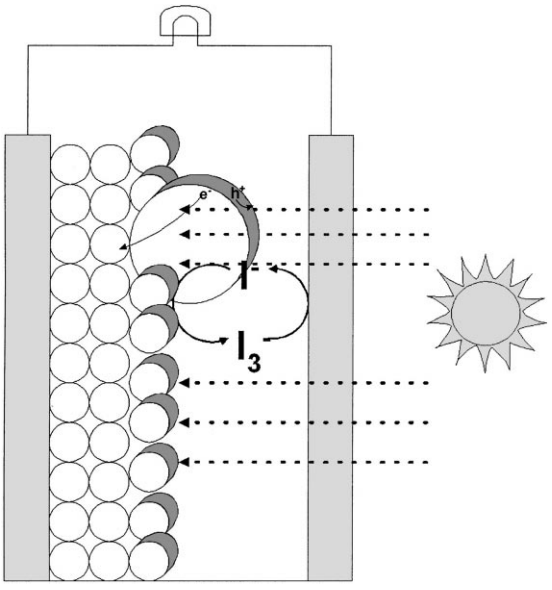

Fig. 1. Schematic representation of dye-sensitized photoelectrochemical photovoltaic cells.

charged "hole" slows down considerably the back reaction to produce high quantum efficiency charge separation. The recombination rates were reported to be in the nanoseconds range [17,18].

The mechanism of the electron transport in this system and in particular the particle-particle transport is less clear. Intensity modulated photocurrent spectroscopy (IMPS) and time-resolved photocurrent measurements [19–23] indicates that the interparticle electron transport is rate limiting. The reported diffusion coefficient is around $10^{-6}\,cm^2/s$ [20,21] and changes with light intensity. This is in contrast to the diffusion coefficient of electrons in rutile estimated at $10^{-2}\,cm^2/s$ [20]. The most common approach to account for these observations is that the conduction is dominated by thermally assisted hopping through trap states. Nelson [24] developed a continuous-time random-walk model to account for these observations. The model assumes given energetic trap distribution and assumes that the electrolyte screens out Coulombic forces and allows the electrons to move within the semiconductor in a Brownian diffusion. The model assumes that the traps are localized at the surface with a concentration of $10^{14}\,cm^{-2}$.

3. Photocatalysis

Recent efforts in photocatalysis with semiconducting particles are driven toward practical applications in photocatalytic detoxification [25–31]. Photocatalytic solar detoxification scheme is based on band-gap illumination of materials such as TiO_2 to produce highly potent oxidants (holes) at the semiconductor surface [25–31]. For hydrocarbons, the process may be simply represented as

$$\text{Organic pollutant} + O_2 \underset{\text{photocatalyst}}{\overset{h\nu}{\rightarrow}} CO_2 + H_2O \qquad (1)$$

while for halogenated organic compounds, the process can be described as

$$HRX + O_2 \underset{\text{photocatalyst}}{\overset{h\nu}{\rightarrow}} CO_2 + HX + H_2O \qquad (2)$$

where X is the halogen.

Sufficient supply of oxygen and efficient removal of the oxidation products are essential for these reactions to proceed all the way to the fully "benign" end products ("mineralization" [25–31]). When the reaction is limited by the oxygen supply, alternative reaction routes such as polymerization often take place.

For a variety of specific applications such as cleaning of oil spills, there were attempts to use these materials on solid supports such as glass [33], nafion membrane [34], Clays [35] and similar supports or in sponge form such as aerogels [47–54]. It was observed that the photochemical and photophysical properties could be affected by the support. In particular that the rate limiting step with slurries of semiconductors is the intrinsic rate on the catalyst surface while often on a supported catalyst, the rate limiting step is mass transfer [32].

Either in a supported form or free-standing, nanocrystalline catalytic materials require analysis of the catalytic processes in nanoscale-size restricted geometries. The issue of chemical reactions in restricted geometries is not new and there is now a considerable experimental [36] and theoretical [37–41] activity in this area. Most of the experimental work involves catalysts on insulating supports such as vycor glass, silica gel, membranes and zeolites. The possible correlations between morphologies of catalytic structures and fractals was reviewed by Van Damme [26].

Since the field is still at its infancy, there are relatively few in depth studies of the kinetics of these heterogeneous reactions. In many studies, the kinetics is being parametrized by a langmuirian shape with a slow surface reaction such that the rate is proportional to the surface coverage given by a Langmuir isotherm in the form:

$$\Gamma = \Gamma_{max}\frac{K_{ad}C}{1 + K_{ad}C} \qquad (3)$$

where Γ is the number of molecules per unit surface area and Γ_{max} the maximum number of molecules per unit surface area that can be adsorbed, C the concentration of the reactant and K_{ad} is the adsorption coefficient of the reactant on the illuminated semiconductor [42]. There exists already an extensive database for the rate parameters for various pollutants. Drake et al. [43] found that oxygen quenching of the triplet state of benzophenone on homologous series of silica gels the quenching rate increases linearly with the mean pore diameter. This was discussed in terms of a random walk model for this type of reac-

tion that was earlier proposed by Blumen et al. [44]. This work was done on two series of commercial silica gels, one that was obtained by random packing of nearly identical spheres of various radii and the other with hierarchical growth morphology. These supports were characterized in terms of BET surface area (gas not specified) and mean pore size. The kinetics were correlated with the mean pore size.

Wang et al. [45,46] reported that there is an optimal particle size for photooxidation of chloroform on nanocrystalline TiO_2. For an intrinsic TiO_2 they found it to be around 10 nm. This optimum was attributed to the optimum in surface reaction vs. e^-/h^+ recombination. They checked such an optimum with Fe^{+3} and with Nb^{+5}/Pt doped particles. The introduction of Fe^{+3} was based on the idea of using these ions as shallow traps thus affecting the e^-/h^+through selective trapping and detrapping. The Nb^{+5} combination was introduced in the larger particles apparently as electronic dopants that would change the electric field distribution. In both cases they found that the optimal doping concentration changes with particle size.

Systems of particular interest to the author are the aerogels. Aerogels are highly porous materials that are produced via sol–gel processing and supercritical drying. The very high surface area and pore volume of aerogels makes them attractive candidates for catalytic applications. The morphology of the TiO_2 aerogels has been characterized in terms of two length scales. Typical morphology constitutes of 5 nm diameter, rough, crystalline nanoparticles of anatase closely packed into mesoaggregates near 50 nm in size. The mesoaggregates are, in turn, packed to a loosely linked structure with an overall porosity of 80%. The total surface area of these aerogels is attributed to the sum of the surfaces of the nanoparticles [47–54]. Schematic representation of this structure is given in Fig. 2 [50,51].

This morphology was determined by using a variety of techniques that include SANS (small angle neutron scattering), NAI (nitrogen adsorption isotherm (measures the pore distribution)), TEM (transmission electron microscopy), SEM (scanning electron microscopy), BET (Brunauer–Emmett–Teller isotherm N_2 adsorption) and XRD (X-ray diffraction**).**One of the key findings of this work can be seen in Figs. 3 and 4 that show the dependence of the quantum efficiency for the photodecomposition of salicylic acid

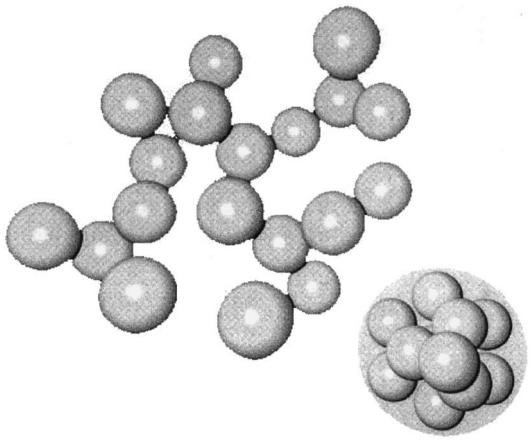

Fig. 2. Schematic representation of the structure of TiO_2 aerogel [51].

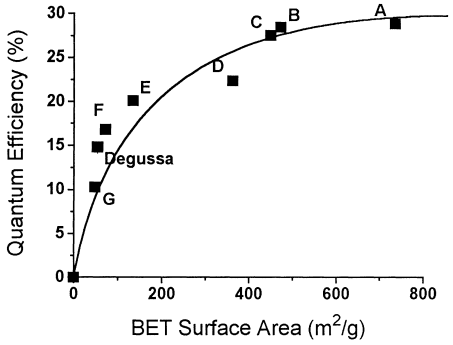

Fig. 3. Quantum efficiencies for photodecomposition of Salicylic Acid on TiO_2 aerogels, as a function of the surface area [52].

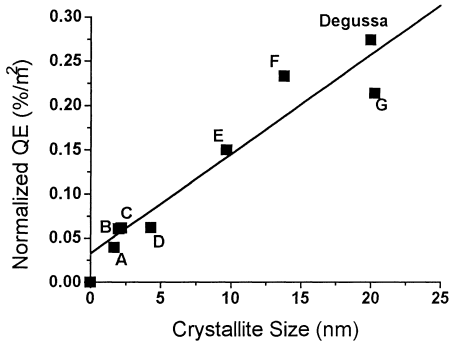

Fig. 4. Quantum efficiencies per unit surface area for photodecomposition of salicylic acid on TiO_2 aerogels, as a function of particle size [52].

on the total surface area and the dependence of the quantum efficiency/surface area on the size of the nanocrystallites [52,53].

While relatively simple scaling arguments that are based on subdividing constant mass mesospheres with finer-grained nanospheres can explain some aspects of these relationships, it becomes clear that the most likely cause for the size dependence is the difficulty of penetration of the substrate into the mesospheres. Since the light absorption takes place in the bulk of the mesospheres, all the photons that are being absorbed by nanoparticles in the interior of the mesosphere, where there is very small substrate adsorption, which generate electron/hole pairs that have to diffuse to the surface of the mesosphere to interact with the substrate. The ratio of nanospheres at the surface of the mesosphere to the total number of nanospheres will determine the fraction of light-induced charge carriers that needs to hop between nanospheres to reach the substrate.

4. Light induced wetting properties

UV illumination of TiO_2 can create a surface that allows both water and oil to spread on a common ground [55–58]. The light induced change from a hydrophobic to a hydrophilic surface was explained initially by light-induced oxidation of traces of oleophilic organic materials that were adsorbed. However, more recent APM and FTIR investigations [55] provided evidence that the generation of the amphiphilic surface is due to the reversible light-induced reduction of Ti^{+4} to Ti^{+3} that can preferentially adsorb hydroxyl groups. The reduced sites can be reoxidized by air to regain the original hydrophobicity. The light-induced surface reduction creates an alternating distribution of hydrophilic and oleophilic regions at the scale of several tens of nanometer. Ultrasonic radiation of the amphiphilic surface greatly facilitates the amphiphilic to hydrophobic reconvertion [58]. This surface chemistry was observed on single crystalline TiO_2 and on polycrystalline TiO_2 deposited on various substrates. This property was found to be of primary commercial importance due to the antifogging and self-cleaning properties of the deposits. The technology is now penetrating various commercial applications, particularly in Japan.

One of the fascinating aspects of this mechanism is the creation of a light-induced critical length scale that is independent of the underlying morphology.

The correlation between this mechanism and the reported changes of the contact angle with roughness [59,60] needs further exploration.

5. Transport

The issue of transport in nanocrystalline systems that is limited by interparticle hopping is obviously of major importance in a variety of applications and is not limited to photovoltaic devices. One of the most fundamental issues is the pathway of the transport; does it take place through the bulk of the crystallites or through the surface. Taking grain boundary of 0.5 nm in a 5 nm diameter particle, the volume ratio between surface and bulk is approximately 1:1 decreasing as $1/r$ with the size of the particle.

The issue was analyzed experimentally by Chiang et al. [61] by investigating transport on nanometer size CeO_{2-x}. This is a convenient material since mechanism of electronic conductivity is dominated by small polarons, the mean free path is on the order of atomic separation and the carrier mobility is not determined by scattering from the interfaces. In addition, it appears that in this case the grain boundaries are crystalline and not amorphous.

Fig. 5, taken from their paper, shows comparison of impedance spectra of a course-grained oxide (a) and the nanocrystalline material (b). Two semicircles: one due to the bulk and the other due to the interfaces are clearly seen in the spectrum of the course-grained material. Only one semicircle, due to the interfaces, is observed in the nanocrystalline material. This finding strongly suggests predominance of conduction through the interface in nanocrystalline materials. They found that the resistance per grain boundary is three orders of magnitude lower in the nanocrystalline material compared with the microcrystalline material and they found that the electronic conductivity is four orders of magnitude greater for the nanocrystals than the one expected from extrapolation of the conductivity of the microcrystalline material. They attribute the difference to size-dependent grain boundary impurity segregation. Similar results were reported for nanocrystalline TiO_2 [62].

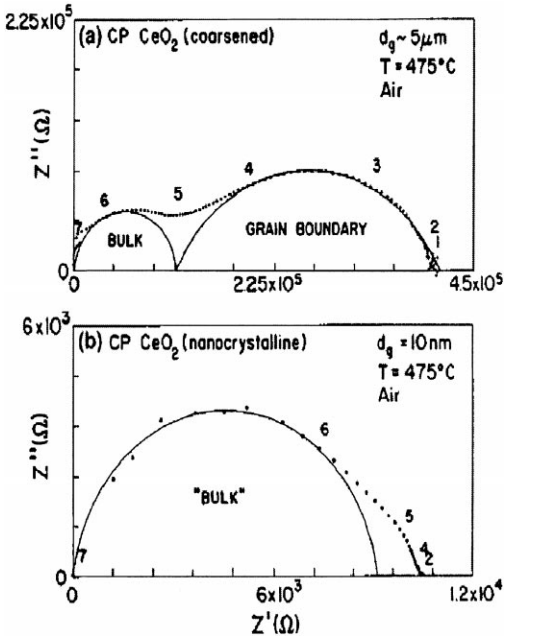

Fig. 5. Impedance spectra for (a) coarse-grained and (b) nanocrystalline ceria, showing a reduced low-frequency arc for blocking grain boundaries in the latter [61].

Significant amount of effort to address this issue is focused on attempts to understand the dielectric properties of porous Si. He et al. [63] addresses the same issue in the context of the conduction properties of porous Si. They address the issue of the conductivity of nc-Si:H nanoparticles of approximate 5 nm grain size with 1 nm grain boundary of amorphous Si embedded in SiO_2. They use Two-Phase Random Composite Effective Medium Theory to distinguish between the contributions of the bulk and the interface. Their results show that the relative high conductivity of porous Si comes from the crystalline bulk while the interface region can be regarded as an insulator. The conductivity increases exponentially with the atomic fraction of the crystalline component and decreases with grain size. The electronic tunneling between the grains is a thermally assisted process through the grain boundary barriers. Cruz et al. [64] applied time dependent tight binding model to calculate the rate of carriers hopping between isolated pairs of c-Si dots embedded in SiO_2. The geometry was modeled as a percolation cluster. They describe the process as a trap controlled hopping process.

6. Polarization

Huong and Birman [65] were the first to predict the existence of internal polarization in CdSe nanoparticles due to a piezoelectric effect caused by the strain between the nanocrystals and ZnS capping layer. Blanton et al. [66] were able to measure the size-dependent permanent dipole of CdSe by measuring the dielectric dispersion of a suspension of monodispersed CdSe particles in hexane and analyzing the results according to the Debye-Onsager equation of the dielectric response due to dilute concentration of spherical dipoles after discounting contributions from net-charged nanocrystallites.

They found a good agreement between the measured result and expected correlation with the internal polarization:

$$P_0 = \mu \frac{(2\varepsilon_1 + \varepsilon_2)}{4\pi a^3 \varepsilon_1} \tag{4}$$

where P_0 is the internal polarization taken as $0.6\,\mu C/cm^2$, π the dipole moment, ε_1 the dielectric constant of the surrounding matrix, ε_2 the dielectric constant of the semiconducting nanoparticle and a the radius of the particle.

The potential drop across the particle was calculated as

$$\Delta\phi = \frac{2\mu\varepsilon_1}{a^2} \tag{5}$$

The dipole moments for CdSe particles were found to be 25D for 1.7 nm particles and 47D for the 2.3 nm particles. The potential drop across both size particles was found to be 0.25 V. If one takes Eqs. (4) and (5), apply them to 5 nm TiO_2 particles, assuming similar P_0 to CdSe, one gets dipole moments in vacuum and water to be 22.5D and 600D, respectively, while the potential drop will be 0.22 V in both cases.

Rabani et al. [67] suggested that the dipole moment originated from lifting of the inversion symmetry in a hexagonal lattice and is extremely sensitive to the structure of the nanocrystal. In a recent publication Shim and Guyof-Sinnest [68] discusses the possible origin of the polarization and concludes that it cannot

originate from the stress since it is independent of the capping. Admitting that more work is required to ascertain the origin of the polarization, they support surface-charge as the most plausible mechanism for the polarization. Recently, Jackson et al. [69] used first principled, density-functional theory to calculate electric polarizabilities and dipole moments of Si clusters and found that the polarizabilities of the clusters are larger than the bulk limit based on the Clausius–Mossotti relation.

7. Adsorption

Within the context of photocatalysis, nanocrystallinity was initially approached as an extension of high surface area [32] catalysis in which the usual competition between adsorption on active sites and diffusion of reactants and products from the active sites take place. As was mentioned before, the need to satisfy simultaneously more than one length scale raised the possibility that the optimum morphology should be fractal with self-similarity over some appropriate range [4]. At sub-monolayer coverage adsorption was shown to follow the Langmuir isotherm (1).

However, recently it was shown that the two parameters of the isotherm, the adsorption coefficient and the maximum number of molecules per unit surface area are probably size and structure dependent in mesoscopic materials.

Zheng et al. [70] investigated the size dependence of the adsorption coefficient taking into account the variation of surface tension with particle size. They arrived at the following expression that describes the ratio of the adsorption coefficients of particles of different sizes:

$$\frac{K_{\mathrm{ad}}(r_1)}{K_{\mathrm{ad}}(r_2)} = \exp\left\{\frac{V_{\mathrm{m}}\left[\gamma_{0(s-1)} - \gamma_{0(\mathrm{s})}\right]}{RT} \times \left[\frac{1}{r_1} f\left(\frac{\delta}{r_1}\right) - \frac{1}{r_2} f\left(\frac{\delta}{r_2}\right)\right]\right\} \quad (6)$$

where V_{m} is the molar volume, $\gamma_{0(s-1)}$and $\gamma_{0(s)}$ are the interfacial tension of macroscopic particles with and without adsorbing species, r_1 and r_2 are the particle radii and δ the thickness of the grain boundary. The function $f(\delta/r)$ was approximated by a regression function. The behavior was experimentally verified on adsorption of organic acids on 6 and 16 nm TiO_2 particles. $\Gamma_{\max}$ was found to be approximately constant, independent of size and independent of the adsorbate. The ratio of the adsorption constants, $K_{\mathrm{ad}}(6\,\mathrm{nm})/K_{\mathrm{ad}}(16\,\mathrm{nm})$, varies between 3.4 for acetic acid and 70 for adipic acid.

Bavykin et al. [71] noticed a sharp size-dependence of the absorption coefficient of methyl viologene on sulfur ion rich CdS nanoparticles. Cd^{++} enriched particles do not show such a dependence.

8. Limits

Throughout this paper we have discussed some of the changes that take place in the physical and chemical properties of semiconducting photocatalysts as they approach sizes of a few unit cells. A central topic in this discussion is the relative role of surface vs. bulk. Exact boundaries between the two do not exist, however, as we have demonstrated in a number of cases, these boundaries enter almost every theoretical attempt to quantify these changes. All of this requires some understanding about limits to smallness. Sun and Lu [72] show that there is thermodynamically based grain size limit for crystalline materials below which the amorphous state is energetically favored. They showed experimentally, on Se crystallites, that the enthalpy of crystallization varies linearly with $1/d$, where d is the average grain size. The extrapolated value to zero enthalpy difference was defined as the minimum grain size below which the amorphous state is energetically favored.

References

[1] E.A. Chandross, R.D. Miller, Chem. Rev. 99 (1999) 1641.
[2] G.S. McCarty, P.S. Weiss, Chem. Rev. 99 (1999) 1983.
[3] A.P. Alivisatos, J. Phys. Chem. 100 (1996) 13226.
[4] R. Gutfraind, M. Sheintuch, D. Avnir, J. Phys. Chem. 95 (1991) 6100.
[5] M. Smart, R. Willhalm, S. Mori, Chemical Economic Handbook, Vol. 1000A, p. 599.
[6] Corma, Chem. Rev. 97 (1997) 2373.
[7] N. Gfeller, S. Megelski, G. Calzaferri, J. Phys. Chem. B 102 (1998) 2433.
[8] L.E. Brus, Appl. Phys. A 53 (1991) 465.

[9] D.J. Norris, M.G. Bawendi, Science 271 (1996) 933.
[10] S.A. Empedocles, Phys. Rev. Lett. 77 (1996) 18.
[11] B. O'Regan, M. Grätzel, Nature 353 (1991) 737.
[12] X. Hagfelds, B. Didriksson, T. Palmqvist, H. Lindström, S. Södergen, H. Rensmo, S.E. Lindquist, Solar Energy Mater. Solar Cells 31 (1994) 481.
[13] M. Grätzel, K. kalyanasundaram, Cur. Sci. 66 (1994) 706.
[14] M. Grätzel, Semiconductor nanoclusters, in: P.V. Kamat, D. Meisel (Eds.), Studies in Surface Science and Catalysis, Vol. 103, Elsevier, Amsterdam, 1995.
[15] M. Grätzel, in: Proceedings of the DOE Workshop on Research Opportunities in Photochemical Sciences, 1996.
[16] R.J. Ellington, J.B. Asbury, S. Ferrere, H.N. Ghosh, J.R. Sprague, T. Lian, A.J. Nozik, J. Phys. Chem. 102 (1998) 6455.
[17] T. Hannappel, B.W. Storck, F. Willig, J. Phys. Chem. 101 (1997) 6799.
[18] Y. Tachibana, J.E. Moser, M. Grätzel, D.R. Klug, J.R. Durrant, J. Phys. Chem. 100 (1996) 20 056.
[19] K. Schschwarzburg, F. Willig, Appl. Phys. Lett. 58 (1991) 2520.
[20] K.F. Cao, G Oskam, G.J. Meyer, P.C. Searson, J. Phys. Chem. 100 (1996) 17021.
[21] L. Dloczik, O. Heperuma, I. Lauermann, L.M. Peter, E.A. Ponomarev, G. Redmond, N.J. Shaw, I. Uhlendorf, J. Phys. Chem B 101 (1997) 10281.
[22] G. Franco, J. Gehring, L.M. Peter, E.A. Ponomarev, I. Uhledorf, J. Phys. Chem. B 103 (1999) 692.
[23] P.E. de Jongh, D. Vanmaekelbergh, J. Phys. Chem B 101 (1997) 2716.
[24] J. Nelson, Phys. Rev. B. 59 (1999) 15374.
[25] M. Schavello (Ed.), Photocatalysis and Enviroment Trends and Applications, Vol. 237, NATO ASI Series C, Kluwer, Dordrecht, The Netherland, 1988.
[26] H. Van Damme, Photocatalysis — Fundamentals and Applications, Wiley, New York, 1989, p. 175.
[27] E. Pelizzetti, E. Minero, V. Maurino, Adv. Coll. In. 32 (1990) 271.
[28] M.R. Hoffmann, S.T. Martin, W. Choi, D.W. Bahnemann, Chem. Rev. 95 (1995) 69.
[29] P.V. Kamat, Chem. Rev. 93 (1993) 267.
[30] M.A. Fox, M.T. Dulay, Chem. Rev. 93 (1993) 34.
[31] D.F. Ollis, H. Al-Ekabi, Photocatalytic Purification and Treatment of Water and Air, Elsevier, Amsterdam, 1993.
[32] D.F. Ollis, E. Pelizzeti, N. Serpone, in: Ref. [1b]., p. 603.
[33] J. Kuczynki, J.K. Thomas, J. Phys. Chem. 89 (1985) 2720.
[34] N. Kakuta, K.H. Park, M.F. Finlayson, A.J. Bard, A. Campion, M.A. Fox, S.E. Weber, J.M. White, J. Phys. Chem. 89 (1985) 732.
[35] O. Enea, A.J. Bard, J. Phys. Chem. 89 (1985) 3828.
[36] N.J. Turro, Tetrahedron 43 (1987) 1589.
[37] D. Avnir, O. Citri, D. Farin, M. Ottolenghi, A. Seri-Levy, in: P.J. Path (Ed.), Optimal Structures in Heterogeneous Reaction Systems, Springer, Berlin (1990).
[38] K. Lindeberg, B.J. West, R. Kopelman, Phys. Rev. Lett. 60 (1988) 1777.
[39] R.M. Ziff, E. Gulari, Y. Barshad, Phys. Rev. Lett. 56 (1986) 2553.
[40] D. Ben-Avraham, S. Render, D.B. Considine, P. Meakin, J. Phys. A 23 (1990) L613.
[41] M. Sheintuch, S. Baradon, Chem. Eng. Sci. 44 (1989) 69.
[42] N. Kakuta, K.H. Park, M.F. Finlayson, A.J. Bard, A. Campion, M.A. Fox, S.E. Webber, J.M. White, J. Phys. Chem. 89 (1985) 732.
[43] J.M. Drake, P. Levitz, N.J. Turro, K.S. Nitsce, K.F. Cassidy, J. Phys. Chem. 92 (1988) 4680.
[44] A. Blumen, G. Zumofen, J. Klafter, Phys. Rev. B 30 (1984) 5379.
[45] C.C. Wang, Z. Zhang, J.Y. Ying, Nanostr. Mater. 9 (1997) 583.
[46] Z. Zhung, C.C. Wang, R. Zakaria, J.Y. Ying, J. Phys. Chem. B 102 (1998) 10871.
[47] G. Dagan, M. Tomkiewicz, J. Phys. Chem 97 (1993) 12651.
[48] M. Tomkiewicz, G. Dagan, Z. Zhu, Res. Chem. Intermediates 20 (1994) 701.
[49] G. Dagan, M. Tomkiewicz, J. Non-crystalline Solids 175 (1994) 294.
[50] Z. Zhu, L.Y. Tsung, M. Tomkiewicz, J. Phys. Chem. 99 (1995) 15945.
[51] Z. Zhu, M. Lin, G. Dagan, M. Tomkiewicz, J. Phys. Chem. 99 (1995) 15950.
[52] M. Tomkiewicz, S. Kelly, in: E. Pelizzetti (Ed.), Fine Particles Science and Technology. From Micro to Nano Particles, Reidel, Dordrechet, 1996.
[53] M. Tomkiewicz, S. Kelly, Morphology dependent photocatalysis with nanoparticle aggregates, in: Nanoparticles in Solids and Solutions. Preparation, Characterization and Application, VCH, Weinheim, 1997.
[54] S. Kelly, F.H. Pollak, M. Tomkiewicz, J. Phys. Chem. 101 (1997) 2730.
[55] R. Wang, N. Sakai, A. Fujishima, T. Watanabe, Kazuhito Hashimoto, J. Phys. Chem. B 103 (1999) 2188.
[56] R. Wang, K. Hashimoto, A. Fujishima, M. Chikuni, E. Kojima, A. Kitamura, M. Shimohigoshi, T. Watanabe, Nature 388 (1997) 431.
[57] R. Wang, K. Hashimoto, A. Fujishima, M. Chikuni, E. Kojima, A. Kitamura, M. Shimohigoshi, T. Watanabe, Adv. Mater. 10 (1998) 135.
[58] N. Sakai, R. Wang, A. Fujishima, T. Watanabe, K. Hashimoto, Langmuir 14 (1998) 5918.
[59] A.W. Adamson, in: Physical Chemistry of Surfaces, 5th Edition, Wiley, New York, 1990 (Chapter X, Section 4).
[60] T. Onda, S. Shibuichi, N. Satoh, K. Tsujii, Langmuir 12 (1996) 2125.
[61] Y.M. Chiang, E.B. Lavik, I. Kosacki, H.L. Tuller, J.Y. Ying, Appl. Phys. Lett. 69 (1996) 185.
[62] P. Knauth, H.L. Tuller, J. Appl. Phys. 85 (1999) 897.
[63] Y. He, Y. Wei, G. Zheng, M. Ya, M. Liu, J. Appl. Phys. 82 (1997) 3408.
[64] H. Cruz, D. Louis, N.E. Capuj, L. Pavesi, J. Appl. Phys. 83 (1998) 7693.
[65] N.Q. Huong, J.L. Birman, J. Chem. Phys. 5 (1998) 1769.
[66] S.A. Blanton, R.L. Leheny, M.A. Hinesand, P. Guyot-Sionnest, Phys. Rev. Lett. 79 (1997) 865.

[67] E. Rabani, B. Hetenyi, B.J. Berne, L.E. Brus, J. Chem. Phys. 110 (1999) 5355.
[68] M. Shim, P. Guyot-Sionnest, J. Chem. Phys. 111 (1999) 6955.
[69] K. Jackson, M. Pederson, C.-Z. Wang, K.-M. Ho, Phys. Rev. A 59 (1999) 3685.
[70] H. Zheng, R.L. Penn, R.J. Hamers, J.F. Banfield, J. Phys. Chem. B 103 (1999) 4656.
[71] D.V. Bavykin, E.N. Savinov, V.N. Parmon, Langmuir 4722 (1999).
[72] N.Y. Sun, K. Lu, Phys. Rev. B 59 (1999) 5987.